Iranian Journal of Science and Technology, Transactions of Mechanical Engineering (2021) 45:299–309
https://doi.org/10.1007/s40997-020-00401-5

RESEARCH PAPER

Surface Characteristics and Cavitation Damage in 8090Al–Li Alloy by Using Cavitation Water Jet Peening Processing

Joseph Sekyi-Ansah[1] · Yun Wang[1] · James Kwasi Quaisie[1] · Fuzhu Li[1] · Chao Yu[1] · Emmanuel Asamoah[1] · Hong Liu[1]

Received: 6 February 2020 / Accepted: 5 October 2020 / Published online: 21 October 2020

Abstract

The cavitation strengthening test of Aluminum lithium Alloy (8090Al–Li) was carried out with different pressure process parameters. The roughness, residual stress, and morphology of the treated samples were studied**.** A high dislocation density was formed in the cavitation area of the workpiece, which resulted in surfacing hardening. The cavitation effect occurred in the collapse area. It was beneficial for the process to be the right choice for the surface treatment of metal materials. The results confirmed that surface roughness, grain size, micro-strain, erosive effect, and micro-hardness of the alloy were significantly affected by different cavitation peening pressures. In this case, surface roughness increased as the impact pressure increased. Besides, the microcrystalline structure decreased in the cavitation treatment area. The study showed on how the impact of the different cavitation peening pressure could suppress the material surfaces, the compressive residual stress, attained the maximum values of −137 MPa to −162 MPa, which increased from 7.87 to 27.56%, as compared to the original sample. In contrast, the corresponding surface roughness average increased to 3.04 μm. Experimental observation shows that the cavitation collapse boundaries obtained by the proposed sample surface and metallographic images were highly complete and accurate.

Keywords Cavitation water jet peening · Surface layer · Plastic deformation · XRD: crystallite size · Micro-strain

1 Introduction

Cavitation is a physical phenomenon that involves the formation and breakdown of bubbles (gases/vapors) within a liquid because of a drop in pressure. Bubbles are formed, when the pressure of the fluid drops under the vapor pressure, which then increases the pressure bubbles implode, forming liquid microjets and shock waves. Cavitation jet initiator is one of the most familiar cavitation phenomena in a laboratory. In the cavitation jet device, the jet was injected with high pressure and high speed in the test room filled with water. This leads to shear cavitation, that can be enhanced by proper design of the pipe nozzle shape through assembly and applying certain hydrodynamic conditions (Hutli et al. 2017; Kumagai et al. 2011).

In recent years, cavitation has assisted in manufacturing, and material synthesis which has been widely reported, in the open literature (Sekyi-Ansah et al. 2020) conducted a study using cavitation water jet peening on 8090Al–Li. They observed that the aluminum lithium 8090 alloy has the advantages of high specific strength, lightweight, and good plasticity, which are widely used in the manufacturing of products in the aviation industry. Aluminum alloys are widely used due to their excellent characteristics such as corrosion resistance, light in weight, toughness and so on. Several surface treatments have been conducted using different methods like shot peening, laser shot peening, etc., (Arif 2003; Yilbas et al. 2009, 2004; Yun et al. 2019). Besides, the application of the above methods in the aviation industry has its disadvantages such as pollution, high cost, etc. However, cavitation effects could be considered as damage forms as well as a beneficial process, CWJP is a resource-rich processing method, used to improve properties of materials characteristics. Generally, cavitation damage is a very complicated process. Its characteristics and control values involve a larger number of geometric, hydraulic and chemical factors, as well as material properties. Therefore, the results of the early cavitation damage and erosion tests showed significant variability and were still scattered

✉ Joseph Sekyi-Ansah
joseph.sekyi-ansah@tpoly.edu.gh

[1] School of Mechanical Engineering, Jiangsu University, Zhenjiang 212013, People's Republic of China

by more extensive data (Bordeasu et al. 2010; Hattori et al. 2009; Soyama 2013). The relationship between cavitation strength and material erosion rate can be studied accurately, the critical parameters for predicting cavitation damage and erosion rate in the early stage can be identified (Chahine et al. 2014; Hattori et al. 2006, 2010). The significance of these parameters for cavitation concentration and shedding frequency is deliberated in the literature (Hutli et al. 2016; Soyama 2004). Cavitation collapse (CC) affects microstructure and deformation of the material, which refers to the relatively low-pressure range, the formation of bubbles in a liquid. In contrast, bubbles are generated in the nozzle due to the partial pressure drop of the flowing liquid, thus forming cavities in the material. The implosion or collapse of these bubbles causes a strong shock wave on the surface of the material, causing significant damage to the metal surface and hardening it. With the increase in exposure time, erosion, and crack appear on the surface after treatment. The time required for erosion is called incubation time, and its length is mainly determined by the strength of the material and other influential factors that are supposed to be constant (Hutli et al. 2016; Hutli and Nedeljkovic 2008). The microstructure of the material has a strong effect on their strength and corrosion resistance. The formation of fine grain by the strain of metal is a hotspot of surface enhancement in recent years (Lu et al. 2010). Besides, plastic deformation changes the lattice structure of the surfaces during cavitation water jet shock peening. X-ray diffraction (XRD) measures full-width half maximum (FWHM) depends on the crystal size and micro-strain. In this case, micro-strain depends on plastic deformation due to CWJP.

The purpose of this paper is to study the effect of cavitation peening on pressure induced in the presence of the higher magnitude compressive residual stress on surface morphology, microstructure, and hardness of metal during plastic deformation was studied. In addition, it elaborates on the understanding of the cavitation damage formation and different peening pressure processes using a simplified experimental vision-based approach. A comparison of high and low pressure of the CWJP process and the prominent factors promoting the formation of erosive defect on the sample surfaces, micro-strain, and reduction in crystal size is determined.

2 Material and Methods

2.1 Experimental Material

The sample used in this study was 8090Al–Li alloy plate, which was cut into a 50 mm × 50 mm × 4 mm square. The chemical composition and mechanical properties are shown in Tables 1 and 2. The surfaces of the sample were clean ultrasonically in ethanol before CWJP.

2.2 Experimental Setup

The experiment was performed with the cavitation shot peening equipment developed by the research team. The flow rate of the system was 14 L/min, and the maximum pressure is 50 MPa. The cavitation peening time was set at 20 min, and the distance (S) from the nozzle to the sample surface was 100 mm. The free liquid level at the top of the water tank was 60 cm, and this was to ensure that the cavitating water jet shock peening was not disturbed by the free liquid level. (Fig. 1a, b) shows the experimental device of cavitation impact expansion of water jet. The tap water was stored for 24 h and tested in a large water tank of 23 ± 2 °C. The experiment was carried out in a transparent tank. The nozzle used in this experiment was designed with reference to the angular nozzles, where the throat diameter nozzle d is 1.5 mm, throat length is 12 mm, and expanded angle of 20° as shown in Fig. 2.

3 Results and Discussion

The results presented in this section include morphology examination, X-ray diffraction analysis, and micro-hardness. The findings are listed under appropriate subheadings**.**

3.1 Morphology of the Cavitation-Peened Surface

The surface of the sample has been etched with [HF (5%): HNO_3 (10%): H_2O (85%)]. Cotton was dip and swab into the corrosive liquid and evenly apply it on the surface continuously for the 30 s, after remove it, dip it in water to wash the surface for few minutes and finally dip the sample in ethanol alcohol to clean the surfaces. The affected metallographic corrosive surface roughness area was observed by using the evolution function of laser confocal microscope (OM). Figure 3 confirms the microstructure grain boundaries work-piece surface after cavitation treatment. As confirmed in Fig. 3a, the surface of the sample is smooth with residue, which confirms the polishing effect before the CWJP process. Besides, the microstructure described also indicates oriented grains resulting from rolling operations

Table 1 Mechanical properties of aluminum–lithium 8090 alloy

Mechanical property	Yield stress strength (MPa)	Tensile strength (MPa)	Poisson's ratio (υ)	Elongation (%)	Elastic modulus (GPa)
value	90	300	0.33	13	67

Table 2 Chemical composition of aluminum–lithium 8090 alloy

Element	Al–Li	Cu	Mg	Fe	Zn	Si	Zr	Mn	Cr	Ti	Residual
Mass fraction	2.2–2.7	1.0–1.6	0.6–1.3	0	0.25	0	0.040–0.16	0.1	0	0	0

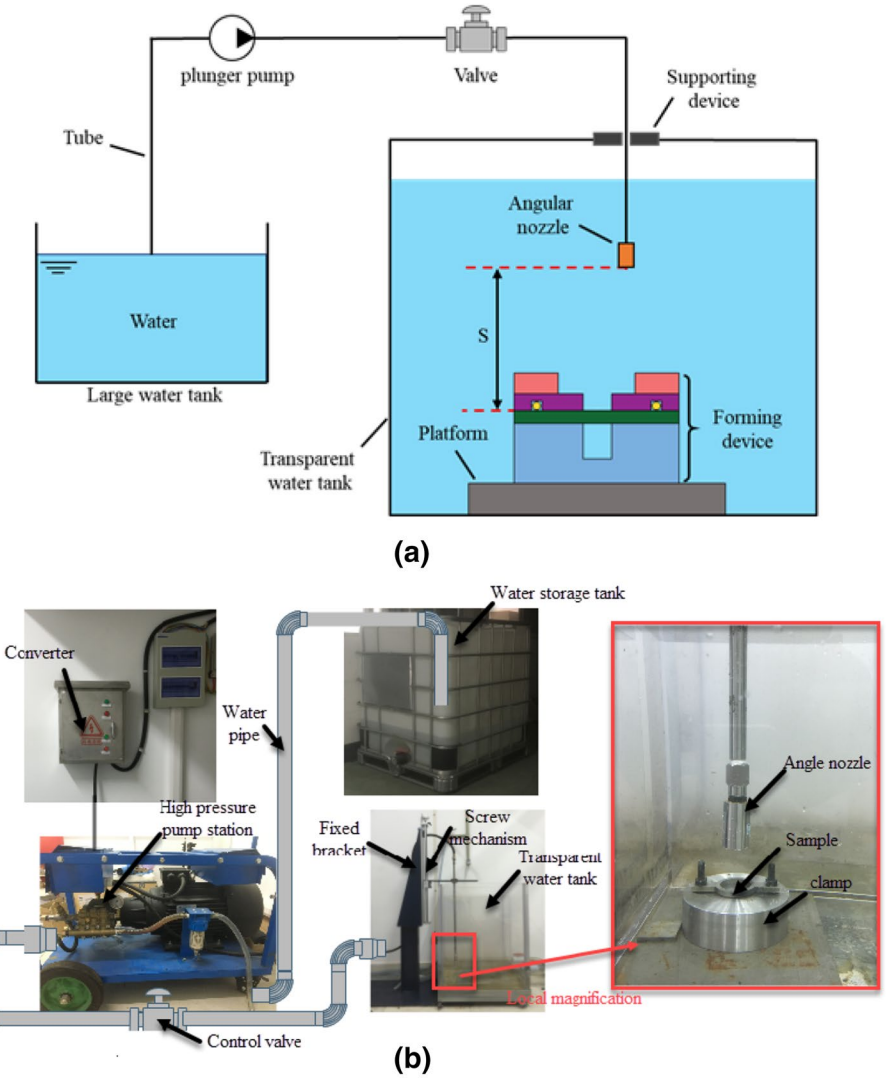

Fig. 1 **a** Water jet cavitation experimental system. **b** Block diagram of water jet cavitation experimental system

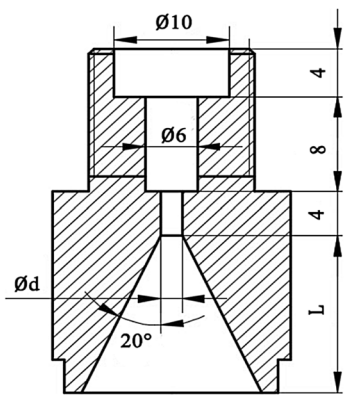

Fig. 2 Nozzle geometry diagram

and precipitated phases in aluminum production, Fig. 3b–d confirm sample images treated with different pressures. The micrograph described shows an uneven surface, possibly due to plastic deformation that occurred during the cavitation water jet peening process and the propagation of the new grain boundary in Fig. 3b–d. The surface morphology of cavitation inhibits the effect on the targeted samples. The etch-peened surface suggests dislocation, where grain refinement was formed on cavitation that occurred on the surface of the workpiece, which confirms a pilling, shallow microstructure grain that occurred on the surface of the target relative to CWJP at a pressure of 20 MPa. In Fig. 3c, when the pressure increases to 25 MPa, the cavitation-peened area of the surface of the microstructure grain size increases.

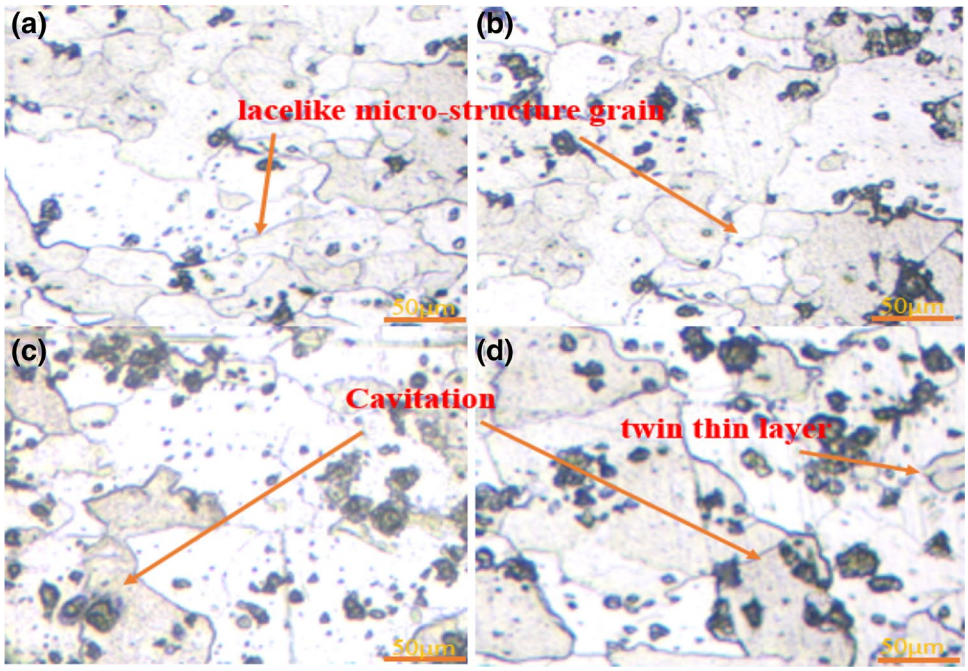

Fig. 3 Microstructure surface layer of different pressure of cavitation water jet peening **a** unpeened; **b** 20 MPa; **c** 25 MPa and **d** 30 MPa

Figure 3d indicates that when the incident pressure increased to 30 MPa, the ablative erosion formed entirely on the workpiece surface. It occurred through vaporization and exposing the lacelike microstructure grain inhibiting in the metallic surface. In Fig. 3d, it could be confirmed that a twin thin layer on the workpiece with cavities and larger microstructure grain, indicating the presence of cavitation collapse effect, grain boundaries, and precipitates that could be identified. It was due to the increase in cavitation peening pressure that causes strain energy to be accumulated effectively, which is also consistent with the observation of the three dimensional (3D) surface morphology mentioned below. Hence, after the cavitation peening, the surface grains deformed, and the grain boundary was blurred. Deformation twins were also seen in the coarse alpha phase grains. Therefore, CWJP has better corrosion resistance, which is due to the high impact of peening pressure on sample surface modification.

After the Cavitation water jet-peening process, the sample surface was cleaned with ethanol. For all the cavitation-treated surfaces, the five locations of the surface roughness (Ra) were measured using the mechanical profiler (KEYENCE, VK-K250), corresponding to the surface distance of the sample. The surface roughness of 8090Al–Li alloy untreated and treated by CWJP is shown in Table 3. The untreated sample had a surface roughness (Ra) of 0.38 μm. After the sample was peened with a pressure of 20 MPa, the roughness value increased to 0.7 μm, indicating that the roughness was doubled as compared with the untreated sample. In other cases, due to the occurrence of bubble rupture, which inhibits the increase in surface vapor. The surface roughness increased gradually with the impact of cavitation-peened pressure from 25 to 30 MPa with their corresponding values of 0.799 μm to 3.04 μm. It was observed from the surface roughness data and SEM photographs that, the surface of the workpiece depressed under compressive stress due to cavitation impact in the CWJP process. Tan et al. (2018) studied cavitation peening behavior on the surface morphology of aluminum 2A12 alloy, and confirmed that the surface roughness increased with the impact of CWJP, whilst Soyama and co, studied the effect of size nozzle pressure. Their results confirmed that the surface roughness of material increased after the cavitation peening (Soyama et al. 2011).

Table 3 Surface roughness (Ra) of 8090Al–Li alloy in different CWJP parameters

Cavitation peening pressure (MPa)	Roughness average (μm)
Unpeened	0.38
20	0.70
25	0.799
30	3.04

3.2 Macro Surface Damaged Morphology and Cavitation Damage Mechanism Analysis

Figure 4 shows the macroscopic morphology of 8090Al–Li before and after CWJP. Figure 4a shows the polished sample before and after CWJP, and the surfaces showed a mirror-like flat surface. Figure 4b–d indicates the various incident

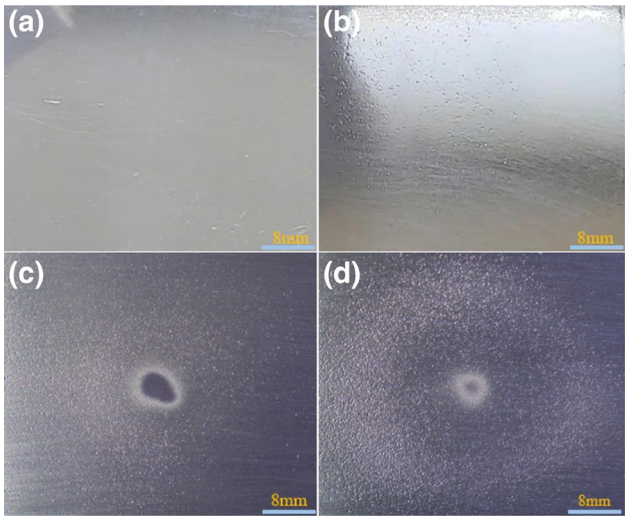

Fig. 4 Macro surface morphology analysis of different cavitation pressure: **a** unpeened; **b** 20 MPa; **c** 25 MPa and **d** 30 MPa

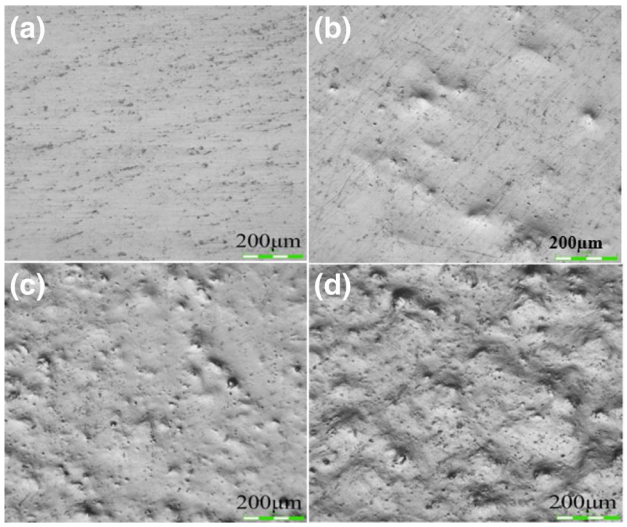

Fig. 5 Roughness morphology of 8090Al–Li samples with different peening pressure **a** unpeened; **b** 20 MPa; **c** 25 MPa, and **d** 30 MPa

pressures (20, 25 and 30 MPa) after cavitation peening. When the sample was peened at a pressure of 20 MPa, the sample surface formed a relatively flat and uniform distribution of pits, which caused a diffuse reflection of light on the material surface. The material surface shows a matte color and the intensity area of matte color increased with the increases of cavitation peening intensity. At the same time, when the pressure was changed to 25 MPa, the sample surface after cavitation peening had an obvious ring with a uniform distribution of a large number of pits and a plastic deformation-strengthening belt, which varied with different peening pressure to cause deformation on the surfaces of the samples. It was mainly due to the cavitation water jet after peening with the indecent pressure of 30 MPa on the surface specimen, which confirmed many cavities were spreading around the specimen surface center area in the ring concentrated zone. The impact was generated by the high-pressure speed droplet collapse bubble zone, which was, as a result of the targeted pressure in the experimental area was in the cavitation zone of the jet flow.

3.3 The Influence of Different Targeted Pressure on the Shot Peening Effect of Cavitating Water Jet

From Fig. 5a could be seen that 8090Al–Li unpeened roughness micro-topography sample surface was smooth, no apparent pits, and dark black dots. It was due to the dark color phenomenon of surface stains in optical digital microscope laser beam irradiation, and the processing nature of the material during manufacturing. But Fig. 5b–d with incident pressures of (20, 25 and 30 MPa), with a constant time of 20 min and a fixed distance of 100 mm on the peened sample, it was confirmed that the pits and the pit density of the sample surface increased when pressure was set to 20 MPa. Besides, the surface roughness value also increased, and further increased when the sample was peened at a pressure of 25 MPa. The plastic deformation increased to an extent, with the increase in the targeted pressure, cavitation water jet peening effect was further strengthened. In contrast, the density of the pit depth of the sample surface increased the surface roughness value when the pressure was set to 30 MPa, as shown in Fig. 5d. The 8090Al–Li sample micro-morphology generated maximum roughness, intense plastic deformation and reflection. The cavitation collapse bubbles, the impact increased the depth of the pit, and some part of the sample surface showed ultimately pitting distribution around the cavitation collapse zone, which belongs to flexible hammer. Still, the deformation surface bumps morphology transition zone coherence, which confirms the effect of cavitation peening was significant.

3.4 Micro-Morphology Cavitation Damage Mechanism Analysis

The surface of the sample has been etched with [HF (5%): HNO_3 (10%): H_2O (85%)]. Cotton was dip and swab into the corrosive liquid and evenly apply it on the surface continuously for the 30 s, after remove it, dip it in water to wash the surface for few minutes and finally dip the sample in ethanol alcohol to clean the surfaces. The affected metallographic corrosive surface roughness area was observed by using the SEM. Figure 6 shows the surface macro-morphology of 8090Al–Li samples after the surface morphology before and after CWJP. In Fig. 6a, the surface shows the original sample, except for a few scratches due to the production of

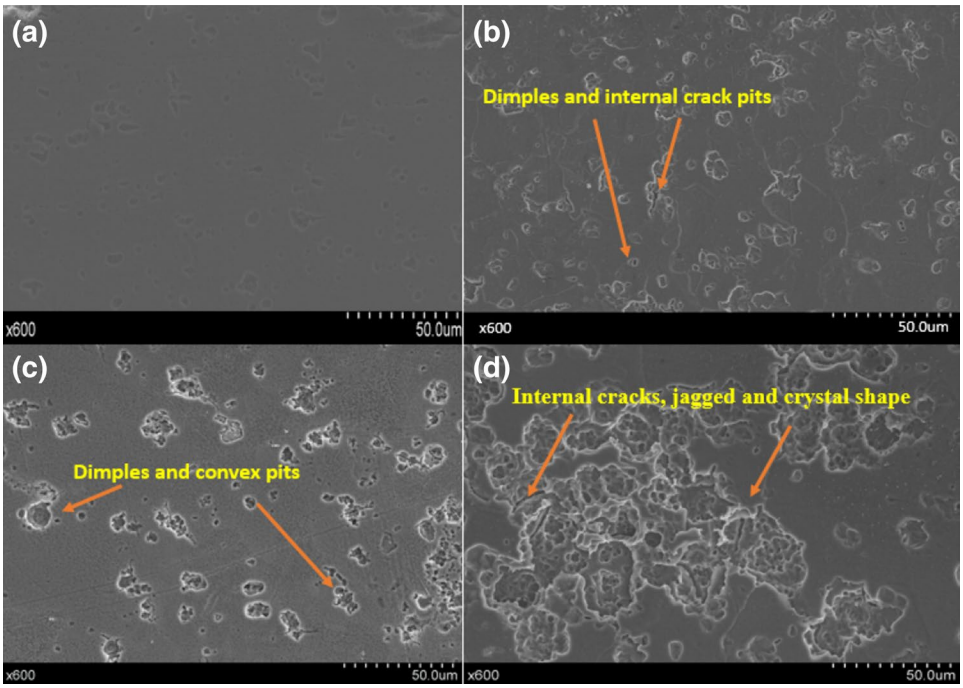

Fig. 6 Microscopic morphology of 8090Al–Li with different peening pressure: **a** unpeened; **b** 20 MPa; **c** 25 MPa and **d** 30 MPa

the material and some reflective outer water stains caused by the edge. Fig. 6b indicates that at a pressure of 20 MPa, a distance of 100 mm and a time of 20 min, the surface plastic deformation between the dimples and pits on the sample surface area occurred due to the peening impact. However, at a pressure of 25 MPa confirms the dumb light in the cavitation bubble collapse pressure affected area under the cavitation impact; the uniform distribution of the sample surface had a large number of the convex pit and plastic deformation strengthening as shown in Fig. 6c. Figure 6d confirms that the high-pressure collapse shock area occurred continuously, showing the cavitation metallographic erosive pit on the materials when the pressure was 30 MPa. It was due to fatigue failure caused by damage phenomenon with similar jagged and crystal shape. Hutli et al. (2019) conducted a study and also confirm that cavitation peening influences erosive pit on the surface of ductile material.

3.5 High Magnification Micro-Morphology Cavitation Damage Mechanism Analysis

After treatment, the cavitation-peened surface sample was further cut by 10 mm × 10 mm using EDM for SEM observation. The cavitated treated surface was further cleaned by ethanol, and the cleaned surface morphology was analyzed by scanning electron microscope (SEM). Figure 7 shows the incident pressure (20, 25 and 30 MPa), fixed time of 20 min and fixed distance of 100 mm, the peening pressure were varied for the state of plastic deformation, SEM observed the 8090Al–Li sample surface before and after cavitation jet peening treatment. Figure 7a shows the sample surface in its original form except that there are few scratches. It was due to the manufacturing process of the material. Figure 7b–d confirms the different prolong peening pressure impact sample surface of the affected area. In Fig. 7b at a pressure of 20 MPa, confirmed that the internal erosive cracks and convex fluctuation were generated and observed in the sample surface, which indicates that the cavitation peening influences material surface area more and more intense, without damaging the sample surface. Also, the plastic deformation had larger residual stress that improved the fatigue life of the sample. Figure 7c shows that at a pressure of 25 MPa, the sample surface still showed a significant plastic deformation. However, in some surface locations had dispersed erosive and white spots scattered around it. This confirms that high cavitation erosion due to cavitation bubble collapses near the wall of the microjet with repeated impact, which indicates that with the different peening pressure, sample surface quality began to deteriorate gradually. Nevertheless, the cavitation pitting was not only depended on the microjet impact but also cause surface damage when cavitation bubble collapse pressure released high-pressure shock wave. Finally, Fig. 7d show that more intense cavitation damage appeared on the treated surface sample at the incident pressure of 30 MPa. The sample surface observed cavitation eroded, jagged edge, and pit surface spreading, which occurred mainly in the convex position. The erosion of pit and plastic deformation increased more than the unpeened sample.

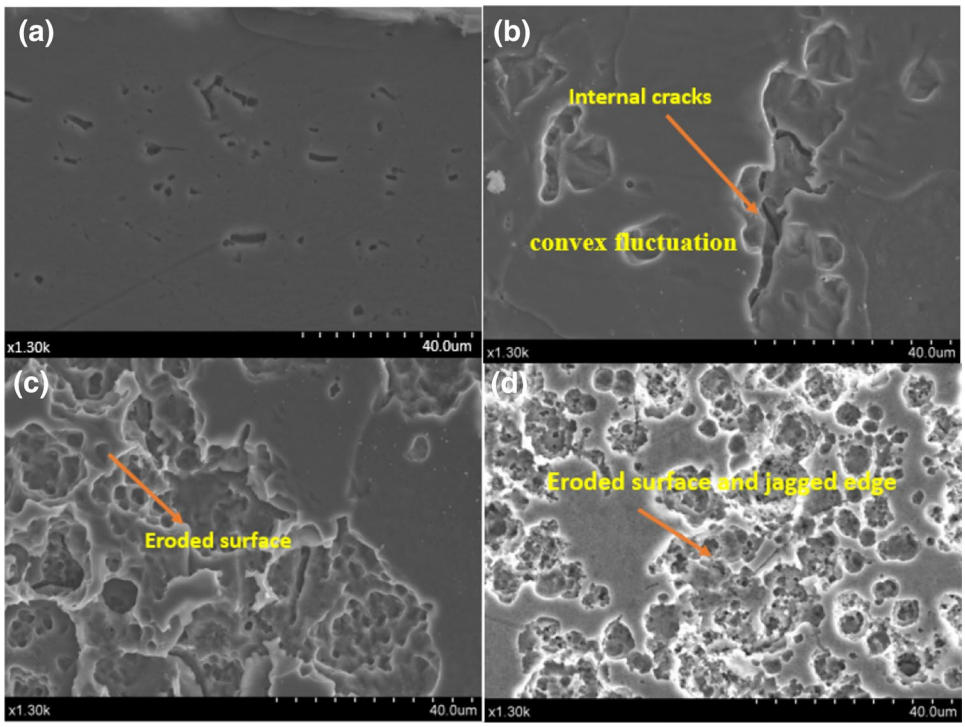

Fig.7 SEM images of 8090Al–Li with different cavitation pressure: **a** unpeened; **b** 20 MPa, **c** 25 MPa and **d** 30 MPa

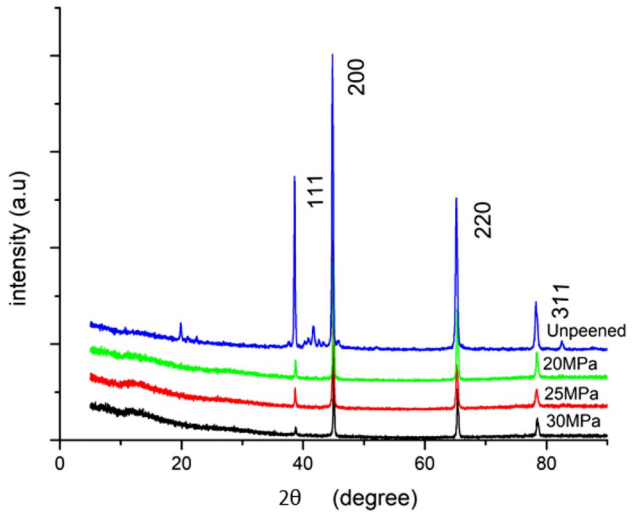

Fig. 8 XRD pattern analysis of peened and unpeened 8090 Al–Li graph

3.6 XRD Analysis

Figure 8 shows the XRD pattern of the specimen before and after CWJP. Most of the diffraction peaks in the XRD pattern of the original sample are $\alpha - Al$ diffraction peaks, only in between (111) and (200) diffraction peaks of $\beta -$ Al appearing at the position of $2\theta \approx 45°$. Also, (200) and (220) also confirmed a twin thin layer $2\theta \approx 50$, which indicated that the surface structure of the original sample was composed of a large number of alpha (α) phases and a small number of beta (β) phases. It was confirmed that the main peak of the sample before and after cavitation peening changed from (111) before cavitation peening to (311), indicating that grain boundary shifted after cavitation peening. Before cavitation peening, due to the influence of polishing, the original sample had preferred and oriented in the diffraction direction of (111), and its peak strength was higher than other peaks. After cavitation peening, the surface absorbed impact pressure energy, which caused the structure of the surface layer to deform, and the diffraction peak of a sample (220) and (311) increased slightly. It was confirmed that compressive residual stress (CRS) induced by peening increased the β phase to the α phase, which was difficult to distinguish in the XRD pattern. The most important characteristic of the XRD pattern was that each diffraction peak of the sample was significantly wide after cavitation peening, which indicated that the surface of the 8090Al–Li alloy after cavitation peening by cavitation water jet had undergone intense plastic deformation

The grain size and lattice micro-strain are calculated by the Scherrer equation (Fultz and Howe 2012) in Eq. (1 and 2)

$$\beta = \frac{k\lambda}{L\cos\theta} \tag{1}$$

$$\beta = C\varepsilon\frac{\sin\theta}{\cos\theta} \tag{2}$$

where the peak width β comprises of the contribution of the crystallite size L and lattice micro-strain. The peak width β is contributed by the microcrystalline (Kanou et al. 2013) size L and lattice micro-strain ε. λ is the wavelength of X-ray and K is the Scherrer constant which is about 1. FWHM is the diffraction peak width in radians, half the height of the background, and the maximum peak. The C value is constant 4, where ε is the inhomogeneous strain. C_ε is a slope of Williamson–Hall plot ($\beta\cos\theta$ vs $\sin\theta$). The change of the structural width of a particular peak reflects the structural change of the diffraction direction in the crystal plane. By using more peaks to calculate the lattice micro-strain and grain size, the change of diffraction direction in different planes could be obtained. This paper uses, $\alpha-$Al (111), (200), (220), and (311) to measure X-ray diffraction peaks and Vickers tester measured micro-hardness distribution of the treated samples. The grain size was significantly refined, and the width was positively correlated with the degree of plastic observed in the metallographic above. Among them, diffraction peaks (111) and (311) of the α phase widened more significantly, which was because the α phase was the largest in Al–Li alloy. The surface where plastic occurred resulted in increased in the more microscopic strain and grain refines. Also, the diffraction peaks of (111), (200), (220) and (311) all shifted to the right to different degrees. Which indicated that the surface spacing of the diffraction crystal plane in the peened sample changed with a CRS inside the sample. It was noted that the XRD diffraction peaks obtained the plotting $\beta\cos\theta$ versus $\sin\theta$. Figure 9 is a schematic diagram of the Williams–hall (W–H) slop. The slope of the Williams–hall curve is known to represent the strain component (ε) (Rai et al. 2004). As the impact pressure increased, the slope curve also increased. According to Eqs. (1) and (2) were obtained from the width of the diffraction peak (β). The diffraction (XRD) was calculated by crystallite size and lattice micro-strain. Related works established on the Scherrer method and W–H plot, testified by Pant et al. (2013), Xu et al. (2019), Min et al. (2004), Sathyajith and Kalainathan (2012). According to Pant et al., selected the largest diffraction single peak and decided the crystal size peaks using the Scherrer method. Pant and co also pointed out that the most accurate results could be obtained by using as many peaks as possible. In our work, crystal sizes and micro-strains were determined using the 5° to 90° range of all diffraction peaks of 2θ. The strain diffraction peak width of hardened materials increased with the increase in average micro-strain and the decreased of grain size generated by plastic deformation (Mordyuk et al. 2008; Woo et al. 2008). In the XRD analysis, the shift of peak was a homogeneity to the strain grains, while the peak width was the heterogeneity of the strain crystals (Fultz and Howe 2012; Pigozzi et al. 2009). Therefore, the plastic deformation and non-uniform strain in the lattice lead to broadening the FWHM of the diffraction peak. The calculated results of grain size and lattice micro-strain of CWJP peened, and unpeened samples are confirmed in Table 4. The surface of the targeted sample increased with the increase in cavitation peening pressure. The experimental results confirmed that the higher the pressure, the smaller the particle grain size. Grain size decreases at high pressure. Under the CWJP condition, the minimum grain size of the workpiece with cavitation peening pressure of 30 MP was 12.82405 nm. To compare with untreated samples, CWJP treatment reduced grain size by 31.31%. In addition, micro-strain increased with the increase in cavitation peening pressure. For the treated samples, the highest micro-strain was obtained. When the pressure was 30 MPa peened compared with unpeened samples, micro-strain increased by 160.98%. The bubbles produced in the CWJP process cause plastic deformation of the surface of the targeted sample. Under the incident pressure of 30 MPa, the deformation zone was superimposed on the treated layer, resulting in a decreased in grain size and an increased in micro-strain. The results confirmed that the larger the pressure, the larger the micro-strain and the smaller the grain size.

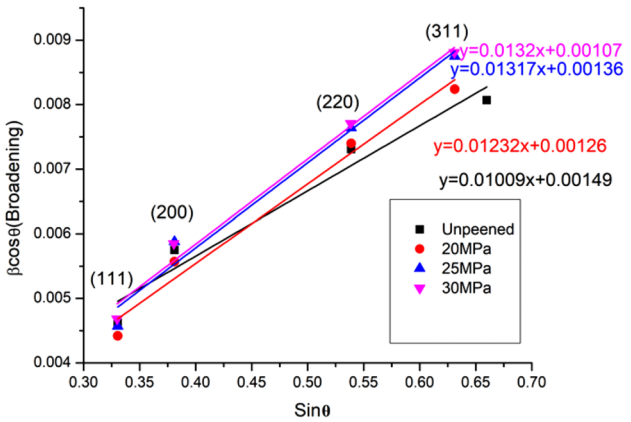

Fig. 9 The Williamson–Hall plots: actual width of XRD diffraction peaks for CWJP peened and unpeened

Table 4 Cavitation peening parameters and the value of crystallite size L and lattice micro-strain ε

Cavitation peening pressure	Crystallite size L (nm)	Lattice micro-strain ε (%)
Unpeened	16.8	11.0
20 MPa	15.9	18.4
25 MPa	15.7	19.5
30 MPa	12.8	28.7

3.7 Micro-hardness

The section of the sample was prepared for hardness tests, and the hardness distribution test of the sample was obtained under 0.5 kg load and 10 s retention time. The measurements were carried out under a series of 50 µm and repeated three times to determine the hardness value of the peened and unpeened conditions. Figure 10 compares the hardness of CWJP peened and unpeened samples. The original sample hardness was 160 HV when it was peened with a pressure of 20 MPa the hardness was 188 HV. In addition, when the pressure was increased to 25 MPa, the hardness increased to 191 HV. The hardness result confirmed that after CWJP treatment, the micro-hardness was significantly improved. In this case, the maximum hardness was 199 HV when the peening pressure was changed to 30 MPa.

This is in very strong accordance with Claurer et al. (1981) experimental results. Reference to the Hall–Petch relationship (Abar et al. 2015; Jia et al. 2014) is that the work-hardening layer can refine the top surface grains of the specimen by enhancing the micro-hardness of the surface. The increase in hardness was due to crystal deformation. Under different peening pressure, the microcrystalline size decreased clearly, and the micro-strain increased. Plastic deformation in the CWJP process leads to strain hardening (Ijiri et al. 2018; Sanchez-Santana et al. 2006; Yilbas et al. 2004). The depth of the deformation layer affected the penetration depth of micro-hardness. Also, it has been reported that the increase in hardness is due to the increase in dislocation density, with an increased in the cavitation peening pressure (Naoe et al. 2010). Bai et al. (2018) confirmed that cavitation peening (CP) produces high-density dislocation and improves the mechanical properties of the metal. In another study, Bail et al. indicated that the micro-hardness of CP decreases gradually with increased depth. They assert that the micro-hardness does not change when the depth exceeds the depth affected by plasticization (Latchoumi et al. 2019). According to the micro-hardness data of the workpiece, the penetration depth of the workpiece after cavitation peening of 30 MPa was higher than that of the workpiece with less peened with CWJP and unpeened.

3.8 Residual Stress

The residual stress measurement layers before and after the CWJP were studied by X-ray diffraction (XRD) $\sin^2 \Psi$ technique. The X-ray beam is 1 mm in diameter and has different positions from 0.0°, 25.0°, 35.0°, and 45.0°. The current, voltage and time to count were 6.0 mA, 22.0 kV and 0.50 s. The diffraction phase is the plane of α (311) and the X-ray source of Cu-K α rays. The scanning of the feed angle was 0.1°/s. The K stress rate is −166 MPa/(°). The starting angle and ending angle of the scanner are set at 136° and 143°. Figure 11 shows the residual stress distribution (RSD) for untreated and different CWJP pressure samples. The results confirmed that the near-surface of the sample which experienced different CWJP plastic deformation, ultimately affected the influence of residual stress (RS) and due to work hardening (Fu et al. 2014). After a peened pressure of 20 MPa, the RS measured value was about −137 MPa at the rear surface of the sample. Residual stress values of −146 MPa and −162 MPa were obtained at 25 MPa and 30 MPa, respectively, affected by the depth of influence of plasticity. When the cavitation pressure was increased from 20 to 30 MPa, the increase rate of RS was about 7.87% to 27.56%. Moreover, the RS attained its saturation point and remained stable as the different cavitation peening pressures increased. Cavitation peening affected the

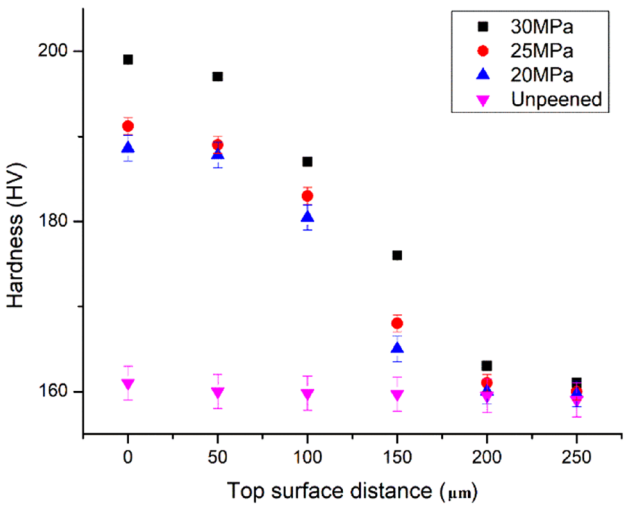

Fig. 10 Micro-hardness profile cross section of the specimen of different pressure

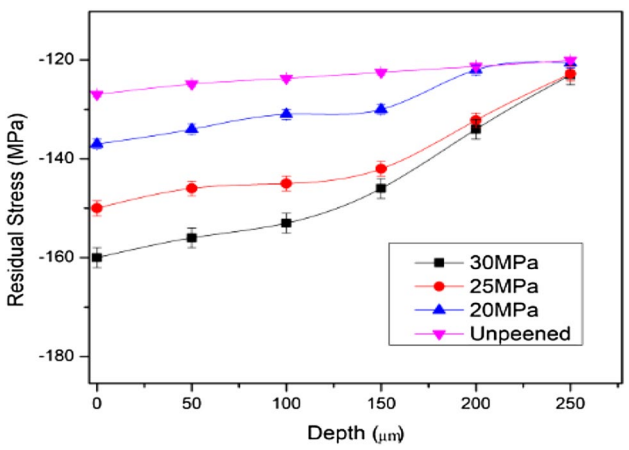

Fig. 11 Residual stress field of 8090 aluminum alloy lithium with different pressure

internal stress caused by an external load. When the stress built up too much in the cavitation area, the fatigue life of the metal could be reduced due to cold working. This indicates that the amount of the affected area is dependent on the RS at the affected depth. (Peyre and Fabbro 1995) investigated the effect of LSP on cast and wrought aluminum alloys on high cycle fatigue (HCF) trends. Their study concluded that the number of LSP impacts affected the high stress levels.

4 Conclusions

The effects of the cavitation water jet peening process and pressure parameters on the surface characteristics of the 8090Al–Li alloy were studied. It was found that at the incident pressure of 20, 25, and 30 MPa had significant effects on the surface roughness, grain size, residual stress, micro-strain, erosive effect, and micro-hardness of 8090Al–Li alloy. When the pressure increased, the surface roughness depth decreased, and the impact strength increased. Delicate crystal structures were formed in the cavitated area. CWJP process leads to the increase in lattice micro-strain and grain size on the surface of the cavitation treated layer. The plastic deformation resulted in grain refinement to about 31.31% and improved the micro-strain to about 160.98%. XRD broadening analysis showed that strain hardening and grain size decreased in the treated area. The hardening layer generated by the pressure of 30 MPa of the CWJP process accounts for about 24.38% of the treated layer to the unpeened sample. With the increase in different pressures, the depth of hardening zone increased. The superposition of processing areas causes a large defect in the immediate area of the workpiece surface, which leads to the micro-plastic deformation of the area. The experimental results confirmed that surface properties of the 8090Al–Li alloy were significantly improved after cavitation treatment.

Acknowledgements The authors are grateful to the project supported by the Natural Science Foundation of China (NSFC, 51575245), Major Research Program of Jiangsu Province (BE2016161), Cultivation project for Academic Leader of Jiangsu Province ([2014] 23), and the members of a cavitation research team in Jiangsu Mechanical department for the helpful comments on this work.

References

Abar F, Abadyan M, Aghazade J (2015) Effects of surface quality and loading history on fatigue life of laser-machined poly (methyl methacrylate). Mater Des 1980–2015(65):473–481

Arif AFM (2003) Numerical prediction of plastic deformation and residual stresses induced by laser shock processing. J Mater Process Technol 136(1–3):120–138

Bai F, Saalbach K-A, Wang L, Wang X, Twiefel J (2018) Impact of time on ultrasonic cavitation peening via detection of surface plastic deformation. Ultrasonics 84:350–355. https://doi.org/10.1016/j.ultras.2017.12.001

Bordeasu I, Popoviciu M, Balasoiu V, Jurchela A, Karabenciov A (2010) Influence of the vibratory test facility type and parameters upon the cavitation erosion evolution. Paper presented at the IOP conference series: earth and environmental science

Chahine GL, Franc J-P, Karimi A (2014) Cavitation and cavitation erosion. In: Kim K-H, Chahine G, Franc J-P, Karimi A (eds) Advanced experimental and numerical techniques for cavitation erosion prediction. Springer, Dordrecht, pp 3–20

Clauer AH, Holbrook JH, Fairand BP (1981) Effects of laser induced shock waves on metals. Shock waves and high-strain-rate phenomena in metals. Springer, New York, pp 675–702

Fu J, Zhu Y, Zheng C, Liu R, Ji Z (2014) Effect of laser shock peening on mechanical properties of Zr-based bulk metallic glass. Appl Surf Sci 313:692–697

Fultz B, Howe JM (2012) Transmission electron microscopy and diffractometry of materials. Springer, New York

Hattori S, Goto Y, Fukuyama T (2006) Influence of temperature on erosion by a cavitating liquid jet. Wear 260(11):1217–1223. https://doi.org/10.1016/j.wear.2005.08.001

Hattori S, Hirose T, Sugiyama K (2009) Prediction method for cavitation erosion based on measurement of bubble collapse impact loads. Paper presented at the journal of physics: conference series.

Hattori S, Hirose T, Sugiyama K (2010) Prediction method for cavitation erosion based on measurement of bubble collapse impact loads. Wear 269(7–8):507–514

Hutli E, Bonyár A, Oszetzky D, Nedeljkovic MS (2016) Plastic deformation and modification of surface characteristics in nano-and micro-levels and enhancement of electric field of FCC materials using cavitation phenomenon. Mech Mater 92:289–298

Hutli E, Fekete T, Nedeljkovic M (2019) Surface characteristics and cavitation damage progress in ductile materials. Eng Fail Anal 106:104157. https://doi.org/10.1016/j.engfailanal.2019.104157

Hutli E, Nedeljkovic MS, Bonyár A, Légrády D (2017) Experimental study on the influence of geometrical parameters on the cavitation erosion characteristics of high speed submerged jets. Exp Therm Fluid Sci 80:281–292

Hutli EA, Nedeljkovic MS (2008) Frequency in shedding/discharging cavitation clouds determined by visualization of a submerged cavitating jet. J Fluids Eng 130(2):021304

Ijiri M, Shimonishi D, Nakagawa D, Yoshimura T (2018) New water jet cavitation technology to increase number and size of cavitation bubbles and its effect on pure Al surface. Int J Lightweight Mater Manuf 1(1):12–20. https://doi.org/10.1016/j.ijlmm.2018.03.003

Jia W, Hong Q, Zhao H, Li L, Han D (2014) Effect of laser shock peening on the mechanical properties of a near-α titanium alloy. Mater Sci Eng A 606:354–359

Kanou S, Nishikawa M, Soyama H (2013) Analysis of the formation of plastic deformation layer on the surface of polycrystalline metals subjected to a micro-size high-rate shot impact. Int J Mech Sci 75:316–323. https://doi.org/10.1016/j.ijmecsci.2013.07.014

Kumagai K, Ryu S, Fujishima K, Kazama T, Ke J (2011) Evaluation of cavitation erosion under submerged jet with CFD. Paper presented at the eighth JFPS international symposium on fluid power.

Latchoumi TP, Balamurugan K, Dinesh K, Ezhilarasi TP (2019) Particle swarm optimization approach for waterjet cavitation peening. Measurement 141:184–189. https://doi.org/10.1016/j.measurement.2019.04.040

Lu J, Luo K, Zhang Y, Cui C, Sun G, Zhou J et al (2010) Grain refinement of LY2 aluminum alloy induced by ultra-high plastic strain during multiple laser shock processing impacts. Acta Mater 58(11):3984–3994

Min KS, Kim KJ, Nam SW (2004) Investigation of the effect of the types and densities of grain boundary carbides on grain boundary cavitation resistance of AISI 321 stainless steel under

creep-fatigue interaction. J Alloys Compd 370(1):223–229. https://doi.org/10.1016/j.jallcom.2003.09.129

Mordyuk B, Milman YV, Iefimov M, Prokopenko G, Silberschmidt V, Danylenko M, Kotko A (2008) Characterization of ultrasonically peened and laser-shock peened surface layers of AISI 321 stainless steel. Surf Coat Technol 202(19):4875–4883

Naoe T, Kogawa H, Yamaguchi Y, Futakawa M (2010) Effect of tensile stress on cavitation damage formation in mercury. J Nucl Mater 398(1):199–206. https://doi.org/10.1016/j.jnucmat.2009.10.033

Pant B, Sundar R, Kumar H, Kaul R, Pavan A, Ranganathan K et al (2013) Studies towards development of laser peening technology for martensitic stainless steel and titanium alloys for steam turbine applications. Mater Sci Eng A 587:352–358

Peyre P, Fabbro R (1995) Laser shock processing: a review of the physics and applications. Opt Quantum Electron 27(12):1213–1229

Pigozzi G, Mukherji D, Gilles R, Jencus P, Siemers C (2009) The measurement of internal strain in core–shell Ni_3Si (Al)–SiO_x nanoparticles. Nanotechnology 20(24):245704

Rai SK, Kumar A, Shankar V, Jayakumar T, Rao KBS, Raj B (2004) Characterization of microstructures in Inconel 625 using X-ray diffraction peak broadening and lattice parameter measurements. Scr Mater 51(1):59–63

Sanchez-Santana U, Rubio-Gonzalez C, Gomez-Rosas G, Ocana J, Molpeceres C, Porro J, Morales M (2006) Wear and friction of 6061-T6 aluminum alloy treated by laser shock processing. Wear 260(7–8):847–854

Sathyajith S, Kalainathan S (2012) Effect of laser shot peening on precipitation hardened aluminum alloy 6061-T6 using low energy laser. Opt Lasers Eng 50(3):345–348

Sekyi-Ansah J, Wang Y, Tan Z, Zhu J, Li F (2020) The dynamic evolution of cavitation vacuolar cloud with high-speed camera. Arabian J Sci Eng. https://doi.org/10.1007/s13369-019-04329-0

Soyama H (2004) Introduction of compressive residual stress using a cavitating jet in air. J Eng Mater Technol 126(1):123–128

Soyama H (2013) Effect of nozzle geometry on a standard cavitation erosion test using a cavitating jet. Wear 297(1–2):895–902

Soyama H, Takakuwa O, Naito A (2011) Effect of injection pressure and size of nozzle throat of a cavitating jet on cavitation peening. Paper presented at the proceedings of 11th international conference on shot peening.

Tan Z, Wang Y, Li F, Li R, Yu C, Fan H, Wang J (2018) Numerical simulation of cavitation behavior and peening experiments in cavitation peening processing. J Phys Conf Ser 1064:012043. https://doi.org/10.1088/1742-6596/1064/1/012043

Woo W, Balogh L, Ungár T, Choo H, Feng Z (2008) Grain structure and dislocation density measurements in a friction-stir welded aluminum alloy using X-ray peak profile analysis. Mater Sci Eng A 498(1–2):308–313

Xu J, Zhang SK, Lu XL, Jiang S, Munroe P, Xie Z-H (2019) Effect of Al alloying on cavitation erosion behavior of $TaSi_2$ nanocrystalline coatings. Ultrason Sonochem 59:104742. https://doi.org/10.1016/j.ultsonch.2019.104742

Yilbas B, Arif A, Karatas C, Raza K (2009) Laser treatment of aluminum surface: analysis of thermal stress field in the irradiated region. J Mater Process Technol 209(1):77–88

Yilbas B, Arif A, Shuja S, Gondal M, Shirokof J (2004) Investigation into laser shock processing. J Mater Eng Perform 13(1):47–54

Yun W, Philip B, Zhenying X, Junfeng W (2019) Study on fatigue crack growth performance of EH36 weldments by laser shock processing. Surf Interfaces 15:199–204. https://doi.org/10.1016/j.surfin.2018.10.009